

# Study of hybrid stars with nonstrange quark matter cores

Cheng-Ming Li<sup>1,\*</sup>, He-Rui Zheng<sup>1</sup>, Shu-Yu Zuo<sup>2</sup>, Ya-Peng Zhao<sup>3,†</sup>, Fei Wang<sup>1</sup>, and Yong-Feng Huang<sup>4</sup>

<sup>1</sup> *Institute for Astrophysics, School of Physics, Zhengzhou University, Zhengzhou 450001, China*

<sup>2</sup> *College of Science, Henan University of Technology, Zhengzhou 450000, China*

<sup>3</sup> *School of Mathematics and Physics, Henan Urban Construction University, Pingdingshan 467036, China and*

<sup>4</sup> *School of Astronomy and Space Science, Nanjing University, Nanjing 210023, China*

In this work, under the hypothesis that quark matter may not be strange [Phys. Rev. Lett. 120, 222001 (2018)], we adopt a modification of the coupling constant of the four-quark scalar interaction  $G \rightarrow G_1 + G_2 \langle \bar{\psi}\psi \rangle$  in the 2-flavor Nambu-Jona-Lasinio model to study nonstrange hybrid stars. According to lattice QCD simulation results of the critical temperature at zero chemical potential,  $G_1$  and  $G_2$  are constrained as  $G_1 \in (1.935, 1.972) \text{ GeV}^{-2}$ , and  $G_2 \in (-1.582, -0.743) \text{ GeV}^{-5}$ , respectively. To obtain hybrid equation of states, the Maxwell construction is used to describe the first-order confinement-deconfinement phase transition in hybrid stars. With recent measurements on neutron star mass, radius, and tidal deformability, the hybrid equation of states are constrained. The result suggests that pure nonstrange quark matter cores can exist in hybrid stars, possessing 0.014-0.026 solar mass with the bag constant  $B^{1/4}$  in a range of 148-161 MeV. It is argued that the binary neutron stars in GW170817 should be hadron stars.

Key-words: hybrid star, Nambu-Jona-Lasinio model, equation of state, Maxwell construction

PACS Numbers: 12.38.Lg, 25.75.Nq, 21.65.Mn

## I. INTRODUCTION

The binary neutron star (BNS) merger GW170817 opens a new era of multi-messenger astronomy [1–23]. More and more astronomical observations on neutron stars arise, facilitating the study of neutron star structure and equation of state (EOS). As natural laboratories to investigate the dense strongly interacting matter, neutron stars have been attracting much attention in astrophysics and theoretical physics. In general, the characteristic temperature of neutron stars can be well described by zero temperature approximation, due to their excessively high energy density in the interior, thus the quantum chromodynamics (QCD) needs to be employed to study the EOS in neutron stars. It is believed that the density in the core of neutron stars could reach 5-10  $\rho_0$ , where  $\rho_0 = 0.16 \text{ fm}^{-3}$  is the nuclear saturation density [24, 25]. As a result, the hadron-quark phase transition is very likely to happen and the deconfined quark matter will appear. In this case, neutron stars are essentially hybrid stars. However, it is difficult to give a unified description of the hadronic matter, quark matter and the hadron-quark phase transition with a single theoretical framework. Thus the hadronic matter and quark matter in hybrid stars are separately described with different EOSs at present, and a certain construction scheme needs to be employed to combine them to get a complete EOS.

As we know, the results of different effective models can be quantitatively or even qualitatively different. Even for the same model, if different modifications are taken into

account, the results can also be different. For example, Fig. 10 of Ref. [26] shows that the EOSs given by different effective models are different from each other, and the corresponding mass-radius ( $M - R$ ) relations of neutron stars are also different. Thus there is not a definite answer to the EOS of dense strongly interacting matter at zero temperature at present.

To describe the hadronic matter in hybrid stars, the Hartree-Fock-Bogoliubov (HFB) mass model HFB-21 with unconventional Skyrme forces called BSK21 [27–30] is a good approach, and the corresponding hadronic EOS obtained in this framework is consistent with current constraints on neutron star masses, radii, and the tidal deformability from GW170817 [31]. However, to describe the quark matter in hybrid stars, the lattice QCD is confronted with difficulties at low-temperature and high-density regions because of the “sign problem”, thus we need to use effective models, such as the Nambu-Jona-Lasinio (NJL) model [32–37], which manifests the spontaneous breaking of chiral symmetry.

In the framework of the NJL-type model, many studies focused on hybrid stars [38–41], aiming to explain the observed two-solar-mass ( $2 M_\odot$ ) compact stars. In Refs. [38–40], the 2-flavor NJL-type model was used to consider the scalar quark-antiquark interaction, anti-triplet scalar diquark interactions and vector quark-antiquark interactions [38], a chemical potential dependence of the vector mean-field coupling  $\eta(\mu)$  and a chemical potential-dependent bag constant  $B(\mu)$  [39], multi-quark (4- and 8-quark) interactions [40], respectively. In Ref. [41], the 3-flavor SU(3) NJL model was adopted with the four-quark scalar, vector-isoscalar and vector-isovector interactions as well as the 't Hooft interaction. Different from the above studies, here we adopt a modification of the coupling constant of four-quark scalar inter-

\* licm@zzu.edu.cn

† zhaoyapeng2013@hotmail.com

actions as  $G \rightarrow G_1 + G_2 \langle \bar{\psi}\psi \rangle$  in this work, which can be regarded as a representation of an effective gluon propagator (See Sec. II for specific analysis).

As for the hadron-quark phase transition, the most widely used approach is the Maxwell construction [42–44], assuming that the first-order phase transition occurs [45, 46] and stable quark matter cores exist in hybrid stars. However, many studies showed that hybrid stars are unstable against oscillations in this case, because star masses decrease with the increase of the central density, thus quark matter cores may not exist in neutron-star interiors [47–49]. In Ref. [47] and Ref. [48], the theoretical modeling of bursting neutron-star spectra and top-down holographic model for strongly interacting quark matter were employed, respectively, to demonstrate that the  $2 M_\odot$  neutron star has ruled out soft EOSs of neutron-star matter, and no quark matter exists in massive neutron stars. Recently, it has been argued that as the density increases, the boundaries of hadrons disappear gradually and the corresponding phase transition is a crossover [50]. According to this assumption, the three-window modeling [51, 52] in the crossover region was proposed. Many studies has constructed hybrid EOSs in this scheme, and the corresponding maximum masses of hybrid stars are compatible with  $2 M_\odot$  [49, 53–57].

In addition to theoretical studies of hadron-quark phase transitions and hybrid EOSs, astronomical observations of neutron star masses, radii, and tidal deformability have also placed constraints on numerous EOSs. Some massive neutron star observations such as PSR J0348+0432 [58] and PSR J0740+6620 [59] require EOSs should not be too soft, but the tidal deformability constrained in BNS merger event GW170817 indicates the EOSs should not be too stiff [1, 60]. Recently, the joint  $M - R$  observations of neutron stars from NASA’s Neutron Star Interior Composition Explorer (NICER) missions have also imposed some constraints on these EOSs [61–64]. In Refs. [65, 66], the authors claim that the gravitational-wave (GW) emission of GW170817 supports a first-order hadron-quark phase transition at supranuclear densities.

In this work, inspired by a recent work that the quark matter may not be strange [67], we will study nonstrange hybrid EOSs and hybrid stars with the Maxwell construction. The hadronic EOS and quark EOS are described by the HFB mass model BSK21 and a modified 2-flavor NJL model, respectively. The parameter space of  $G_1$  and  $G_2$  in the modified NJL model will be fixed according to the lattice results at zero chemical potential [68]. With recent measurements on neutron star mass, radii, and tidal deformability, the hybrid EOSs will be constrained to get the parameter space of the bag constant  $B^{1/4}$ . To ensure that hybrid stars are stable against oscillations, maximum masses of hybrid stars and the masses of their quark matter cores are determined.

It is known that the Bayesian analysis is a good approach to constrain the EOSs. Researchers have obtained important information about the EOS of QCD in this

way [38–41, 69–72]. However, considering that the Lagrangian of the NJL model is convenient for numerical calculation, in this work we have performed calculations focusing on the EOS to get the corresponding hybrid star  $M - R$  relations and tidal deformability, and then compared them with the relevant neutron star astronomical observations. The model parameters and properties of hybrid stars are constrained as well.

This paper is organized as follows. In Sec. II, the modified NJL model for nonstrange quark matter is briefly introduced, and the EOSs of quark matter are derived. In Sec. III, the Maxwell construction is used to get hybrid EOSs. With recent astronomical observations of neutron star mass, radius, and tidal deformability, we constrain the hybrid EOSs. For comparison, the  $M - R$  relations and tidal deformability results of hybrid stars from six representative hybrid EOSs are presented. Finally, a brief summary is given in Sec. IV.

## II. EOS OF NONSTRANGE QUARK MATTER

As an effective model to describe cold dense quark matter, the NJL model [32, 33] is widely used in the study of hybrid stars and quark stars. The general form of the 2-flavor NJL model Lagrangian is:

$$\mathcal{L} = \bar{\psi}(i\not{\partial} - m)\psi + G[(\bar{\psi}\psi)^2 + (\bar{\psi}i\gamma^5\tau\psi)^2], \quad (1)$$

where  $m$  is the current quark mass (because of an exact isospin symmetry between  $u$  and  $d$  quarks adopted in this work,  $m_u = m_d = m$ ), and  $G$  represents the four-fermion coupling constant. The term  $G[(\bar{\psi}\psi)^2 + (\bar{\psi}i\gamma^5\tau\psi)^2]$  describes interactions in scalar-isoscalar and pseudoscalar-isovector channels.

Then the mean-field thermodynamic potential is

$$\Omega(T, \{\mu_f\}, \{\langle \bar{\psi}\psi \rangle_f\}) = \sum_{f=u,d} (\Omega_{M,f}(T, \mu_f) + 2G \langle \bar{\psi}\psi \rangle_f^2) + const, \quad (2)$$

where  $\langle \bar{\psi}\psi \rangle_f$  is the quark condensate of flavor  $f$ , and  $\Omega_{M,f}$  denotes the contribution of a gas of quasiparticles of flavor  $f$ ,

$$\Omega_{M,f} = -2N_c \int \frac{d^3p}{(2\pi)^3} \{T \ln(1 + \exp(-\frac{1}{T}(E_{p,f} - \mu_f))) + T \ln(1 + \exp(-\frac{1}{T}(E_{p,f} + \mu_f))) + E_{p,f}\}. \quad (3)$$

The effective mass of the constituent quark of flavor  $f$  is now given by

$$M_f = m_f - 4G \langle \bar{\psi}\psi \rangle_f. \quad (4)$$

In a thermodynamically consistent treatment, the quark condensate  $\langle \bar{\psi}\psi \rangle_f$  and the particle number density

$\rho_f$  of flavor  $f$  can be derived from  $\Omega$  as

$$\begin{aligned} \langle \bar{\psi}\psi \rangle_f &= \frac{\partial \Omega}{\partial m_f} \\ &= -2N_c \int \frac{d^3p}{(2\pi)^3} \frac{M_f}{E_{p,f}} [1 - n_{p,f}(T, \mu_f) - \bar{n}_{p,f}(T, \mu_f)], \end{aligned} \quad (5)$$

$$\begin{aligned} \rho_f &= -\frac{\partial \Omega}{\partial \mu_f} \\ &= 2N_c \int \frac{d^3p}{(2\pi)^3} (n_{p,f}(T, \mu_f) - \bar{n}_{p,f}(T, \mu_f)), \end{aligned} \quad (6)$$

where  $E_{p,f} = \sqrt{\vec{p}^2 + M_f^2}$  is the quark on-shell energy of flavor  $f$ , and  $n_{p,f}(T, \mu_f)$ ,  $\bar{n}_{p,f}(T, \mu_f)$  are the Fermi occupation numbers of quarks and antiquarks of flavor  $f$ , respectively, which are defined as

$$n_{p,f}(T, \mu_f) = [\exp^{(E_{p,f} - \mu_f)/T} + 1]^{-1}, \quad (7)$$

$$\bar{n}_{p,f}(T, \mu_f) = [\exp^{(E_{p,f} + \mu_f)/T} + 1]^{-1}. \quad (8)$$

Because the NJL model cannot be renormalized, the proper-time regularization is adopted in the following calculations. In addition, we need to fix the parameter set  $(\Lambda_{UV}, G)$  to fit experimental data ( $f_\pi = 92$  MeV,  $M_\pi = 135$  MeV) at zero temperature and chemical potential. According to the Review of Particle Physics [73], the current quark mass  $m$  is chosen as 3.5 MeV in this work. Then the ultraviolet cutoff  $\Lambda_{UV}$  and coupling constant  $G$  are fixed to be 1324 MeV and  $2.005 \text{ GeV}^{-2}$ , respectively. This procedure is similar to Ref. [32].

Based on our current knowledge of strong interactions, the coupling constant  $G$  in the NJL model can be regarded as a representation of an effective gluon propagator. In light of QCD theory, the quark and gluon propagators should satisfy their respective Dyson-Schwinger (DS) equations, and these two equations are coupled with each other. It is demonstrated that quark propagators in the Nambu phase and Wigner phase are very different from each other [74–76], so it can be inferred that the corresponding gluon propagators in these two phases are also different [77]. However, in the normal NJL model,  $G$  is simplified as a constant, remaining the same in these two phases. In addition, according to simulations of lattice QCD, the gluon propagator should vary with temperature, although its dependence on the chemical potential is still uncertain. In the normal NJL model, as a representation of an effective gluon propagator, the coupling constant  $G$  is “static”, and thus cannot fulfill the requirement of lattice QCD.

In the QCD sum rule approach [78], it is argued that the full Green function can be divided into two parts: the perturbative part and nonperturbative part. The condensates can be expressed as various moments of nonperturbative Green function. As a result, the most general form of the “nonperturbative” gluon propagator is

$$D_{\mu\nu}^{\text{npert}} \equiv D_{\mu\nu}^{\text{full}} - D_{\mu\nu}^{\text{pert}} \equiv c_1 \langle \bar{\psi}\psi \rangle + c_2 \langle G^{\mu\nu} G_{\mu\nu} \rangle + \dots, \quad (9)$$

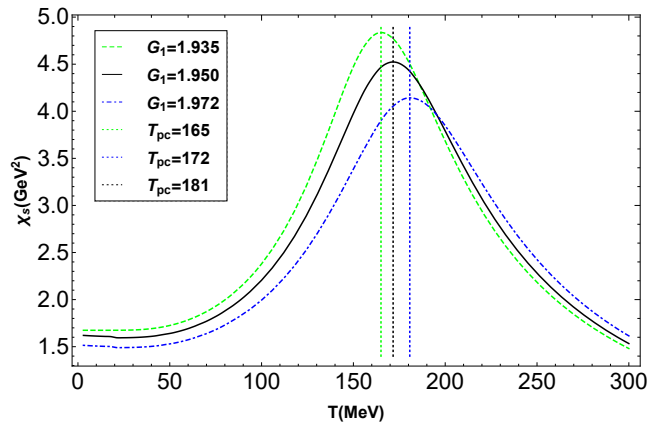


FIG. 1. The chiral susceptibilities  $\chi_s$  versus temperature for the three parameter sets defined in Table I at  $\mu = 0$ . The three vertical lines denote where the peaks of  $\chi_s$  are located, i.e.,  $T_{pc} = 165, 172, 181$  MeV.

where  $\langle G^{\mu\nu} G_{\mu\nu} \rangle$  refers to the gluon condensate,  $c_1$  and  $c_2$  are coefficients which can be calculated in the QCD sum rule approach [79, 80], and the ellipsis represents the contributions from other condensates, such as the mixed quark-gluon condensate. Among these condensates, the quark condensate possesses the lowest dimension, and a nonzero value of it, in the chiral limit, precisely signifies the dynamical chiral symmetry breaking. Therefore, it plays the most important role in the QCD sum rule approach. In this work, we will deal with its contribution separately, and the contribution of other condensates is simplified into the perturbative part of the gluon propagator. In the normal NJL model, it is equivalent to a modification of the coupling constant  $G$  in the following way [55, 81–87],

$$G \rightarrow G_1 + G_2 \langle \bar{\psi}\psi \rangle. \quad (10)$$

Now the coupling strength  $G$  will depend on both  $u$  and  $d$  quark condensates via this modification, where  $G_2$  refers to the weight factor of the influence of the quark propagator on the gluon propagator.

Although the lattice QCD is confronted with the “sign problem” at finite chemical potentials, the simulating results at zero chemical potential can still help us determine the values of  $G_1$  and  $G_2$ . According to the simulations of lattice QCD, the chiral phase transition at zero chemical potential is a crossover, and the corresponding pseudo-critical point is located at  $T_{pc} = 173 \pm 8$  MeV in the 2-flavor case [68]. Different from the meaning of the so-called “critical point” in the case of first-order phase transition, the “pseudo-critical point” here refers to the condition that the crossover occurs, and its position can be identified by the peak of susceptibilities, such as the chiral susceptibility  $\chi_s$  in Ref. [68], which is defined as  $\chi_s = -\partial \langle \bar{\psi}\psi \rangle / \partial m$  [88].

Fig. 1 plots the chiral susceptibilities versus temperature. We can see that if  $G_1$  varies from 1.935 to 1.972

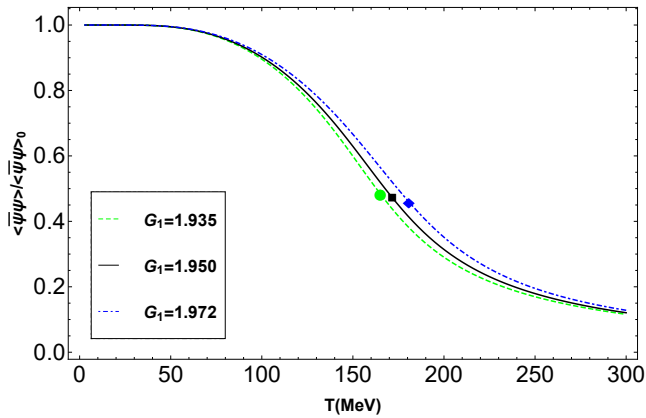


FIG. 2. The scaled quark condensates versus  $T$  for the three parameter sets in Table I at  $\mu = 0$ . The corresponding pseudo-critical points are also marked on these curves, respectively.

TABLE I. Parameter sets in this work.

$m$ [MeV]	$\Lambda_{UV}$ [MeV]	$M_{u,d}$ [MeV]	$-\langle \bar{\psi}\psi \rangle^{\frac{1}{3}}$ [MeV]	$G$ [GeV $^{-2}$ ]	$G_1$ [GeV $^{-2}$ ]	$G_2$ [GeV $^{-5}$ ]
					1.935	-1.582
3.5	1324	180	353	2.005	1.950	-1.242
					1.972	-0.743

GeV $^{-2}$ ,  $T_{pc}$  will vary from 165 to 181 MeV, thus satisfy the constraint from lattice simulations. Considering Eq. (10) at  $T = \mu = 0$ , the corresponding value of  $G_2$  can be derived from  $-1.582$  to  $-0.743$  GeV $^{-5}$ . The whole parameter sets of the modified 2-flavor NJL model in this work are shown in Table I, where in addition to the two boundary values of  $G_1$  that meet the requirement of lattice simulations, we also take the parameter set of  $G_1 = 1.950$  GeV $^{-5}$  into account, in order to study the influence of different parameter sets on the EOSs. Fig. 2 plots the scaled order parameter of chiral phase transition ( $\langle \bar{\psi}\psi \rangle / \langle \bar{\psi}\psi \rangle_0$ ) versus temperature. We can find that  $\langle \bar{\psi}\psi \rangle / \langle \bar{\psi}\psi \rangle_0$  decreases smoothly from one to zero as temperature increases, thus the transition at  $\mu = 0$  is the crossover, consistent with the simulation result of lattice QCD. For the three parameter sets in Table I, the pseudo-critical temperature increases with the increase of  $G_1$ .

Now we extend our calculation to finite chemical potentials at  $T = 0$  to get EOSs of the quark matter. After solving Eq. (4) with the modification of Eq. (10), we can get the dependence of effective quark mass  $M_{u,d}$  on the chemical potential, which is shown in Fig. 3. It can be seen that the chiral phase transition at  $T = 0$  is still a crossover for each parameter set in this work. The pseudo-critical chemical potentials  $\mu_{pc}$ , determined by the chiral susceptibility, are 272, 280, and 293 MeV for the three parameter sets of G1935, G1950 and G1972 defined in Table I, respectively.

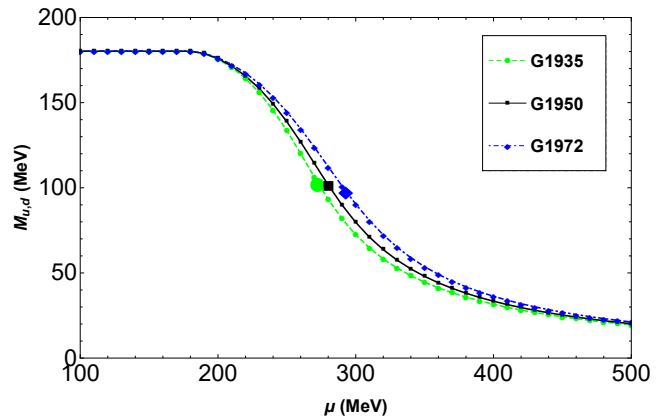


FIG. 3. The effective mass of  $u, d$  quarks versus chemical potentials  $\mu$  at  $T = 0$  for the parameter sets defined in Table I. The marked points on the three lines are the pseudo-critical points with  $\mu_{pc} = 272, 280, 293$  MeV, respectively.

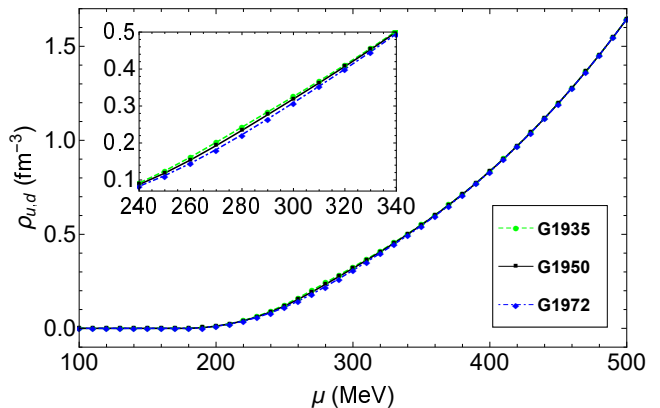


FIG. 4. The number density of  $u, d$  quarks versus chemical potentials  $\mu$  at  $T = 0$  for the parameter sets defined in Table I.

In the framework of the NJL model, it is demonstrated that whether the first-order chiral phase transition occurs at  $T = 0$  (when  $m \neq 0$ ) depends on the regularization scheme that is employed [33, 89, 90]. In Ref. [33], the three-momentum cutoff regularization is used and a first-order phase transition happens at  $T = 0$ . However, in Ref. [89], the authors use the PTR and find a crossover in the phase transition region at  $T = 0$ . Actually, in Ref. [90], it is clarified that the low current quark mass ( $m \leq 4$  MeV) can result in a crossover at  $T = 0$  for both PTR and three-momentum cutoff regularization. It is noted that  $m = 3.5$  MeV in this work just corresponds to the case of low current quark mass, thus a crossover occurs in the chiral phase transition region.

The dependence of quark number density on the chemical potential at  $T = 0$  is shown in Fig. 4. We can see that for the three parameter sets in Table I, the number densities of  $u, d$  quarks are only slightly different in the crossover region, and a smaller value of  $G_1$  corresponds to a larger number density for the same chemical potential.

To describe the strongly interacting matter in hybrid

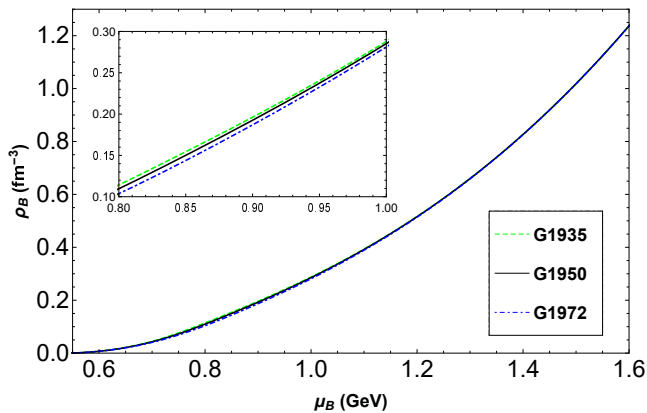


FIG. 5. The baryon density versus baryon chemical potential of the quark system for the parameter sets defined in Table I.

stars, we need to consider the beta equilibrium and electric charge neutrality,

$$\begin{aligned} \mu_d &= \mu_u + \mu_e, \\ \frac{2}{3}\rho_u - \frac{1}{3}\rho_d - \rho_e &= 0, \end{aligned} \quad (11)$$

where  $\rho_e = \mu_e^3/3\pi^2$  is the number density of electrons at  $T = 0$ . For the three parameter sets defined in Table I, the relation between the baryon density  $\rho_B$  and baryon chemical potential  $\mu_B$  is shown in Fig. 5, where  $\mu_B = \mu_u + 2\mu_d$  and  $\rho_B = (\rho_u + \rho_d)/3$ . In Fig. 5, the  $\rho_B - \mu_B$  relations in the cases of  $G_1 = 1.935, 1.950, 1.972 \text{ GeV}^{-2}$  are almost the same except for the crossover region, where a smaller value of  $G_1$  corresponds to a larger  $\rho_B$  for the same  $\mu_B$ .

According to the definition, the EOS of dense quark matter at  $T = 0$  is [91]

$$P(\mu) = P(\mu = 0) + \int_0^\mu d\mu' \rho(\mu'), \quad (12)$$

and the energy density of the quark system can be expressed as [92, 93]

$$\epsilon = -P + \sum_{i=u,d,e} \mu_i \rho_i. \quad (13)$$

It is noted that  $P(\mu = 0)$  in Eq. (14) is irrelevant to the chemical potential. It corresponds to the negative vacuum pressure and cannot be determined in a model-independent way. Just like the vacuum bag constant ( $-B$ ) in the MIT bag model, we treat it as a phenomenological parameter in this work. In general,  $B^{1/4}$  is in a range of 100-200 MeV and should be constrained from ground experiments and astronomical observations [94, 95]. In this work, we will constrain its value in light of recent neutron star observations.

### III. STRUCTURE OF HYBRID STARS

Under the Maxwell construction scheme, the first-order hadron-quark phase transition occurs when the baryon chemical potentials and pressures of these two phases are equal,

$$P_H(\mu_{B,c}) = P_Q(\mu_{B,c}), \quad (14)$$

where  $\mu_{B,c}$  is the critical baryon chemical potential of the hadron-quark phase transition, which is around 1.4 GeV in Fig. 6 for  $G_1 = 1.935, 1.950, 1.972 \text{ GeV}^{-2}$  and  $B^{1/4} = 150, 153, 161 \text{ MeV}$ . Note that the dense hadronic matter in this work is described by the BSK21 parametrization of the Skyrme interaction [27, 28], which is strongly favored by the nuclear-mass measurements [28]. The hybrid EOS can be written as

$$P(\mu_B) = \begin{cases} P_H, & \text{when } \mu_B \leq \mu_{B,c}, \\ P_Q, & \text{when } \mu_B > \mu_{B,c}. \end{cases} \quad (15)$$

The corresponding energy density of the hybrid EOS is

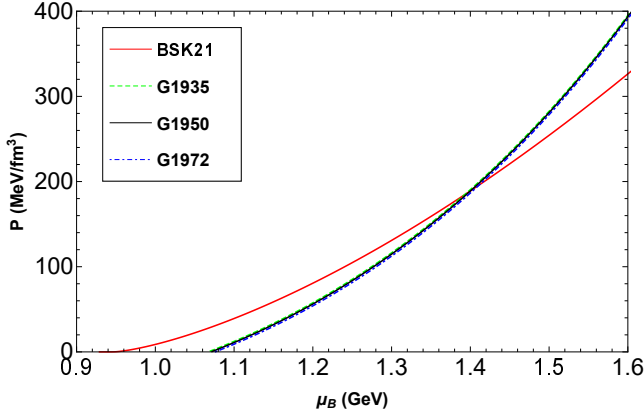
$$\epsilon(\mu_B) = \begin{cases} \epsilon_H, & \text{when } \mu_B \leq \mu_{B,c}, \\ \epsilon_Q, & \text{when } \mu_B > \mu_{B,c}, \end{cases} \quad (16)$$

where  $\epsilon_Q$  is the energy density of the quark system.

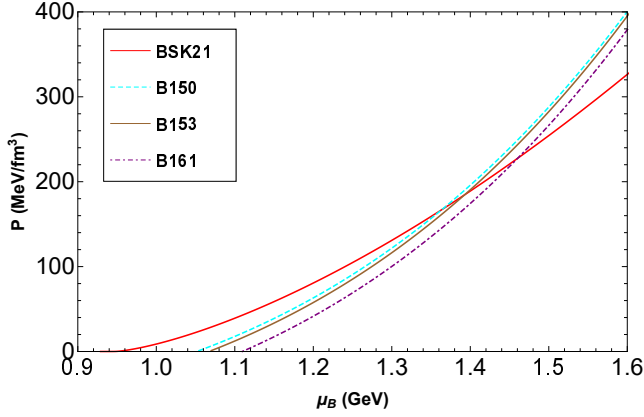
Because  $G_1$  has already been constrained in a range of (1.935, 1.972)  $\text{GeV}^{-2}$  by lattice simulations in Sec. II, the other adjustable parameter  $B^{1/4}$  in hybrid EOSs can be constrained by neutron star observations. In fact, considering the  $2 M_\odot$  constraint, the lower limits of  $B^{1/4}$  in the cases of  $G_1 = 1.935, 1.950, 1.972 \text{ GeV}^{-2}$  should be 150, 149, and 148 MeV, respectively, while the stability of hybrid stars with a quark matter core yields the upper limits of  $B^{1/4}$  as 161, 158, and 157 MeV, respectively. In addition, we will also choose  $B^{1/4} = 153 \text{ MeV}$  for comparison in the following calculation to study the influence of  $B^{1/4}$  on the EOSs and on the structure of hybrid stars.

In Fig. 6, the influences of  $G_1$  and  $B^{1/4}$  on the pressure of the quark matter are presented in the subgraph (a) and (b) with  $B^{1/4} = 153 \text{ MeV}$  and  $G_1 = 1.935 \text{ GeV}^{-2}$ , respectively. When  $B^{1/4} = 153 \text{ MeV}$ , there is little difference between the pressures of the quark matter as long as  $G_1 \in (1.935, 1.972) \text{ GeV}^{-2}$ . However, when  $G_1 = 1.935 \text{ GeV}^{-2}$ , the pressure difference of the quark matter with  $B^{1/4} = 150, 153, 161 \text{ MeV}$  is obvious, and a smaller  $B^{1/4}$  leads to a higher  $P$  for the same  $\mu_B$ .

In Fig. 7, we present the  $\epsilon - P$  relations of the hadronic matter, the quark matter and hybrid EOSs with the Maxwell construction. Each point marked with “x” represents the critical point of the corresponding first-order phase transition, which is denoted with  $(P_{pt}, \epsilon_{pt})$  in the following, and the other marked point on each hybrid EOS refers to the center of the most massive hybrid star, which is denoted with  $(P_c, \epsilon_c)$  in the following. When  $B^{1/4} = 153 \text{ MeV}$ , the locations of  $(P_{pt}, \epsilon_{pt})$  for  $G_1 = 1.935, 1.950 \text{ GeV}^{-2}$  are the same. However, due



(a)



(b)

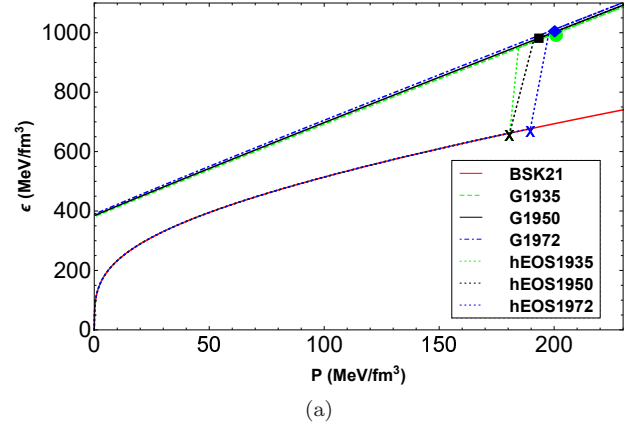
FIG. 6. The pressure versus baryon chemical potential ( $\mu_B$ ) for (a)  $B^{1/4} = 153$  MeV and (b)  $G_1 = 1.935$  GeV $^{-2}$ . The pressure of the hadronic matter described by BSK21 is also presented for a comparison. G1935, G1950, G1972 refer to  $G_1 = 1.935, 1.950, 1.972$  GeV $^{-2}$ , respectively, and B150, B153, B161 refer to  $B^{1/4} = 150, 153, 161$  MeV, respectively.

to the small but non-negligible differences of the hybrid EOSs in these two cases, the corresponding  $(P_c, \epsilon_c)$  are different. When  $G_1 = 1.935$  GeV $^{-2}$ , the differences of both  $(P_{pt}, \epsilon_{pt})$  and  $(P_c, \epsilon_c)$  are obvious in the cases of  $B^{1/4} = 150, 153, 161$  MeV, and a larger  $B^{1/4}$  will lead to larger values of  $(P_{pt}, \epsilon_{pt})$  and  $(P_c, \epsilon_c)$ . The corresponding  $(P_{pt}, \epsilon_{pt})$  and  $(P_c, \epsilon_c)$  points of nine representative hybrid EOSs are listed in Table II.

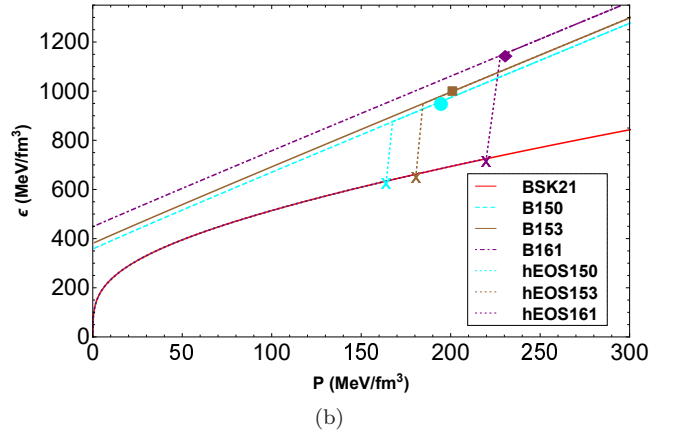
Once the EOS is determined, we can solve the Tolman-Oppenheimer-Volkoff (TOV) equation numerically to get the  $M - R$  and mass-central energy density ( $M - \epsilon_c$ ) relations. In Fig. 8 and Fig. 9, to study the influence of  $G_1$  and  $B^{1/4}$  on the  $M - R$  and  $M - \epsilon_c$  relations, the corresponding results for (a)  $B^{1/4} = 153$  MeV and (b)  $G_1 = 1.935$  GeV $^{-2}$  are shown, respectively. In Fig. 8, the most massive quark star with  $G_1 = 1.935, 1.950, 1.972$  GeV $^{-2}$  ( $B^{1/4} = 150, 153, 161$  MeV) is about  $1.52 M_\odot$  ( $1.57 M_\odot$ ), not satisfying the  $2 M_\odot$  constraint. In addition, the quark stars described by the modified NJL model in this work cannot fulfill the recent  $M - R$  con-

TABLE II. The corresponding  $(P_{pt}, \epsilon_{pt})$  and  $(P_c, \epsilon_c)$  points of nine representative hybrid EOSs.

$G_1$ [GeV $^{-2}$ ]	$B^{1/4}$ [MeV]	$(P_{pt}, \epsilon_{pt})$ [MeV · fm $^{-3}$ ]	$(P_c, \epsilon_c)$ [MeV · fm $^{-3}$ ]
1.935	150	(164.0, 634.1)	(194.6, 957.7)
	153	(180.7, 662.1)	(201.0, 998.9)
	161	(219.9, 725.0)	(230.5, 1153.0)
1.950	149	(164.0, 634.1)	(193.6, 953.6)
	153	(180.7, 662.1)	(193.5, 982.2)
	158	(209.3, 708.4)	(220.9, 1104.6)
1.972	148	(164.0, 634.1)	(194.8, 958.9)
	153	(189.7, 677.0)	(200.2, 1011.3)
	157	(209.3, 708.4)	(220.1, 1102.8)



(a)



(b)

FIG. 7. The  $\epsilon - P$  relation of the quark matter and hybrid EOS when (a)  $B^{1/4} = 153$  MeV and (b)  $G_1 = 1.935$  GeV $^{-2}$ . The  $\epsilon - P$  relation of the hadronic matter described by BSK21 is shown by the red line. G1935, G1950, G1972 (hEOS1935, hEOS1950, hEOS1972) refers to the quark matter (hybrid EOS) when  $G_1 = 1.935, 1.950, 1.972$  GeV $^{-2}$ , respectively, and B150, B153, B161 (hEOS150, hEOS153, hEOS161) refers to quark matter (hybrid EOS) with  $B^{1/4} = 150, 153, 161$  MeV, respectively.

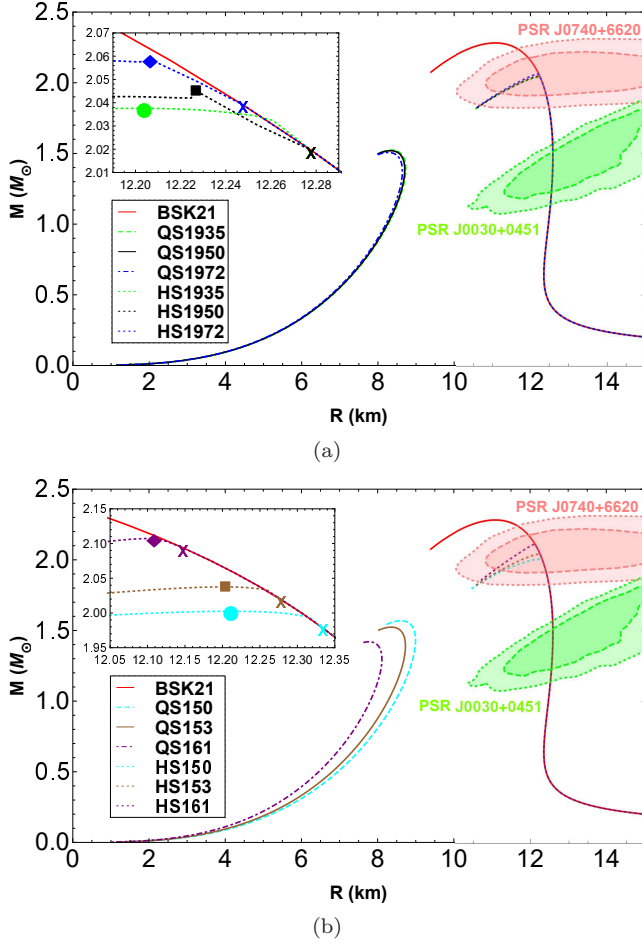


FIG. 8. The  $M - R$  relations of quark stars and hybrid stars for (a)  $B^{1/4} = 153$  MeV and (b)  $G_1 = 1.935$   $\text{GeV}^{-2}$ . The  $M - R$  relation of the hadron star described by BSK21 is shown by the red line. QS1935, QS1950, QS1972 (HS1935, HS1950, HS1972) refer to quark stars (hybrid stars) with  $G_1 = 1.935, 1.950, 1.972$   $\text{GeV}^{-2}$ , respectively, and QS150, QS153, QS161 (HS150, HS153, HS161) refer to quark stars (hybrid stars) with  $B^{1/4} = 150, 153, 161$  MeV, respectively. The constraints from the NICER mission (PSR J0740+6620 [64] and PSR J0030+0451 [62]) are shown as dark (light) colored areas, referring to the 68% (95%) confidence levels.

straint from the NICER mission (PSR J0740+6620 [64] and PSR J0030+0451 [62]). However, the hybrid EOSs obtained with the Maxwell construction approach in this work can produce hybrid stars in consistent with these astronomical observations, although their quark matter cores are relatively small (about  $0.02 M_\odot$ ).

The  $M - \epsilon_c$  relations are shown in Fig. 9. We can find that for stable neutron stars (whether they are hadron stars, quark stars, or hybrid stars), a larger  $\epsilon_c$  corresponds to a more massive star. For different values of  $G_1$ , the  $\epsilon_{\text{pt}}$  ( $\epsilon_c$ ) of the corresponding hybrid stars in the Panel (a) are around 670 (1000)  $\text{MeV}/\text{fm}^3$ , and the difference is very small, which can also be seen in Table II.

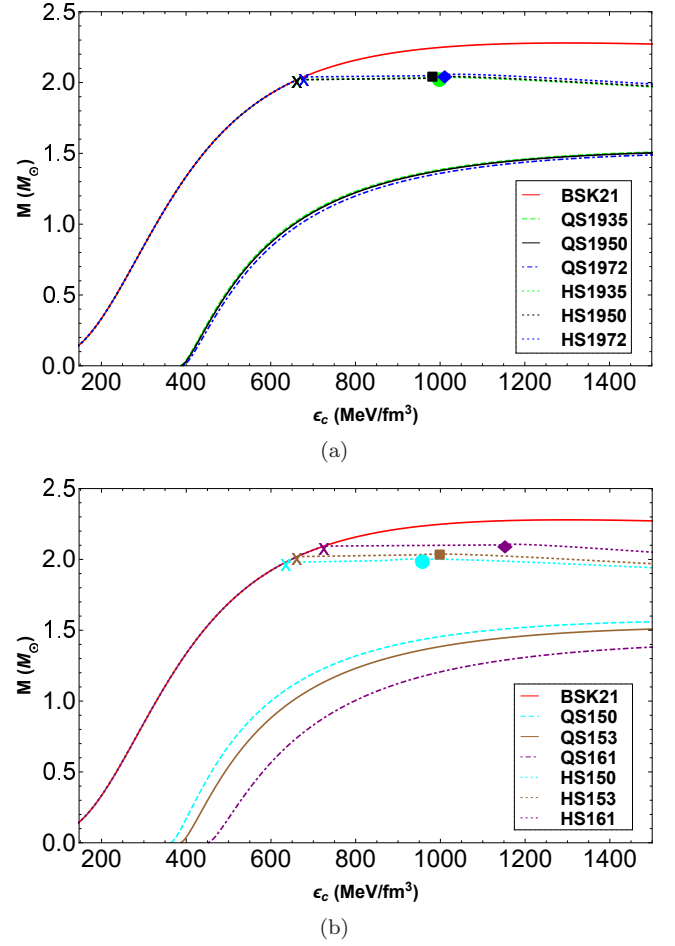


FIG. 9. The  $M - \epsilon_c$  relations of quark stars and hybrid stars for (a)  $B^{1/4} = 153$  MeV and (b)  $G_1 = 1.935$   $\text{GeV}^{-2}$ . The  $M - \epsilon_c$  relation of the hadron star described by BSK21 is shown by the red line. QS1935, QS1950, QS1972 (HS1935, HS1950, HS1972) refer to quark stars (hybrid stars) with  $G_1 = 1.935, 1.950, 1.972$   $\text{GeV}^{-2}$ , respectively, and QS150, QS153, QS161 (HS150, HS153, HS161) refer to quark stars (hybrid stars) with  $B^{1/4} = 150, 153, 161$  MeV, respectively.

In Panel (b), the difference of  $\epsilon_{\text{pt}}$  ( $\epsilon_c$ ) caused by different values of  $B^{1/4}$  is more obvious than that in Panel (a).

We have also calculated the tidal deformability of hadron stars, quark stars and hybrid stars in this work, which is defined as [96],

$$\Lambda = \frac{2}{3} k_2 R^5. \quad (17)$$

Here  $k_2$  is the dimensionless tidal Love number for  $l = 2$ , which can be calculated by

$$\begin{aligned} k_2 = & \frac{8C^5}{5} (1 - 2C)^2 [2 + 2C(y - 1) - y] \\ & \times \{2C[6 - 3y + 3C(5y - 8)] \\ & + 4C^3[13 - 11y + C(3y - 2) + 2C^2(1 + y)] \\ & + 3(1 - 2C)^2 [2 + 2C(y - 1) - y] \ln(1 - 2C)\}^{-1} \end{aligned} \quad (18)$$

where  $C = M/R$  refers to the compactness of the star, and  $y$  is defined as

$$y = R\beta(R)/H(R) - 4\pi R^3\epsilon_0/M, \quad (19)$$

where  $\epsilon_0$  is the energy density at the surface of the star. The dimensionless parameter  $y$  can be calculated by solving the differential equations [96],

$$\begin{aligned} \frac{dH}{dr} &= \beta, \\ \frac{d\beta}{dr} &= 2\left(1 - 2\frac{m_r}{r}\right)^{-1} H \{-2\pi[5\epsilon + 9P + f(\epsilon + P)] \\ &+ \frac{3}{r^2} + 2\left(1 - 2\frac{m_r}{r}\right)^{-1} \left(\frac{m_r}{r^2} + 4\pi r P\right)^2\} \\ &+ \frac{2\beta}{r} \left(1 - 2\frac{m_r}{r}\right)^{-1} \left\{\frac{m_r}{r} + 2\pi r^2(\epsilon - P) - 1\right\}, \end{aligned} \quad (20)$$

where  $H(r)$  is the metric function, and  $f = d\epsilon/dP$ .

The  $\Lambda - M$  relation is shown in Fig. 10. We can see that for quark stars and hadron stars described by the modified NJL model and BSK21 hadronic model, the corresponding values of  $\Lambda(1.4M_\odot)$  satisfy the constraint from GW170817, i.e.,  $\Lambda(1.4M_\odot) = 190_{-120}^{+390}$  [60], except for the quark star with  $G_1 = 1.935 \text{ GeV}^{-2}$  and  $B^{1/4} = 161 \text{ MeV}$ . For stable hybrid stars whose maximum masses are higher than  $2 M_\odot$  in this work, the corresponding hybrid EOSs demonstrate that neutron stars with the masses lower than  $1.98 M_\odot$  are still hadron stars and the quark matter cores do not exist inside them. Therefore, the  $\Lambda - M$  relations from these hybrid EOSs are the same with that of hadron stars when  $M \leq 1.98M_\odot$ , and we do not show  $\Lambda - M$  relations of hybrid stars in Fig. 10. In other words, according to the hybrid EOSs constrained in this work, the BNS in GW170817 whose masses are estimated to be  $1.17\text{-}1.36$  and  $1.36\text{-}1.60 M_\odot$  [1], respectively, should both be hadron stars.

For the sake of completeness, the  $M - R$  properties of hybrid stars constructed by nine representative hybrid EOSs are presented in Table III, where  $(R_{pt}, M_{pt})$  is related to the hadron-quark phase transition point, referring to the radius and mass of the most massive hadron star constructed by the hybrid EOS, and  $(R_{\max}, M_{\max})$  is the radius and mass of the most massive hybrid star with a quark matter core. We can see that the masses of quark matter cores in these nine representative hybrid EOSs are in a range of  $0.014\text{-}0.026 M_\odot$ . When  $B^{1/4} = 153 \text{ MeV}$ , a larger  $G_1$  corresponds to a larger  $M_{\max}$ . For the same  $G_1$ , a larger  $B^{1/4}$  leads to a larger  $M_{pt}$  and  $M_{\max}$ .

#### IV. SUMMARY AND DISCUSSION

In this study, the modified 2-flavor NJL model and the BSK21 parametrization of the Skyrme interaction are introduced to investigate the nonstrange quark matter and hadronic matter in hybrid stars in light of a hypothesis that the quark matter may not be strange. To construct

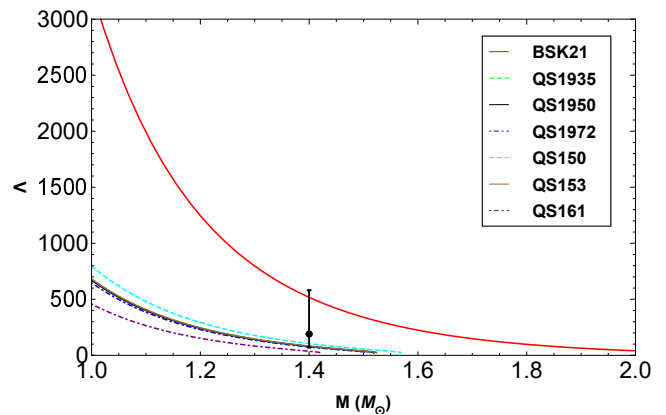


FIG. 10. The  $\Lambda - M$  relation of quark stars and hadron stars. QS1935, QS1950, QS1972 refer to quark stars with  $B^{1/4} = 153 \text{ MeV}$ , and  $G_1 = 1.935, 1.950, 1.972 \text{ GeV}^{-2}$ , respectively, and QS150, QS153, QS161 refer to quark stars with  $G_1 = 1.935 \text{ GeV}^{-2}$ , and  $B^{1/4} = 150, 153, 161 \text{ MeV}$ , respectively. The observational constraint from GW170817 ( $\Lambda(1.4M_\odot) = 190_{-120}^{+390}$  [60]) is also plotted for comparison.

TABLE III. The corresponding  $(R_{pt}, M_{pt})$  and  $(R_{\max}, M_{\max})$  points of nine representative hybrid EOSs.

$G_1$ [GeV $^{-2}$ ]	$B^{1/4}$ [MeV]	$(R_{pt}, M_{pt})$ [km, $M_\odot$ ]	$(R_{\max}, M_{\max})$ [km, $M_\odot$ ]
1.935	150	(12.33, 1.979)	(12.21, 2.002)
	153	(12.28, 2.020)	(12.20, 2.038)
	161	(12.15, 2.094)	(12.11, 2.108)
1.950	149	(12.33, 1.979)	(12.22, 2.002)
	153	(12.28, 2.020)	(12.23, 2.045)
	158	(12.18, 2.076)	(12.14, 2.093)
1.972	148	(12.33, 1.979)	(12.21, 2.005)
	153	(12.25, 2.039)	(12.21, 2.059)
	157	(12.18, 2.076)	(12.14, 2.092)

hybrid EOSs, the first-order hadron-quark phase transition and the corresponding Maxwell construction are considered.

When the current quark mass is chosen as  $m = 3.5 \text{ MeV}$ , which is estimated by the particle data group, the modification of the coupling constant  $G$  in the normal NJL model is helpful, because it is not only consistent with the QCD requirement in essence, but also in agreement with the lattice simulation results of  $T_c$ . In the 2-flavor case when  $T_c = 173 \pm 8 \text{ MeV}$ , our calculations indicate that the parameter space of  $G_1$  is limited to a range of  $1.935\text{-}1.972 \text{ GeV}^{-2}$ , and the corresponding value of  $G_2$  is from  $-1.582$  to  $-0.743 \text{ GeV}^{-5}$ , implying that the normal 2-flavor NJL model with the four-quark scalar interaction (corresponding to the case of  $G_2 = 0$  in our modified NJL model) is inconsistent with the lattice simulation results. For hybrid EOSs, the influence of  $G_1$  is very small, but the influence of  $B^{1/4}$  is obvious.



Considering astronomical observations and the stability of hybrid stars, the parameter  $B^{1/4}$  is constrained to be 150-161, 149-158, 148-157 MeV when  $G_1 = 1.935, 1.950, 1.972 \text{ GeV}^{-2}$ , respectively. The quark EOSs constructed with the modified NJL model in this work is soft, and thus cannot satisfy the  $2 M_\odot$  constraint of neutron stars and the  $M - R$  constraints from NICER missions. It is noted that in some previous studies, the quark matter cores may not exist in compact stars under the Maxwell construction [47–49], or the maximum mass of quark matter cores may be larger than  $0.6 M_\odot$  and the BNS in GW170817 can be hybrid stars [38, 39, 41, 70]. However, with the modified 2-flavor NJL model in this work, the hybrid EOSs with first-order hadron-quark transitions are still in agreement with current neutron star astronomical observations, and pure nonstrange quark matter cores can exist in hybrid stars, possessing a relatively small mass of  $0.014\text{-}0.026 M_\odot$ . According to the hybrid EOSs constrained in this work, the BNS in GW170817 whose masses are estimated to be  $1.17\text{-}1.36$  and  $1.36\text{-}1.60 M_\odot$  [1], respectively, may

be hadron stars.

## ACKNOWLEDGMENTS

This work is supported in part by the national Key Program for Science and Technology Research Development (2023YFB3002500), the National Natural Science Foundation of China (under Grants No. 12005192, No. 12075213, and No. 12233002), the Project funded by China Postdoctoral Science Foundation (No. 2020M672255, No. 2020TQ0287), National SKA Program of China No. 2020SKA0120300, the National Key R&D Program of China (2021YFA0718500), the Natural Science Foundation of Henan Province of China (No. 242300421375), the Natural Science Foundation for Distinguished Young Scholars of Henan Province under grant number 242300421046, the start-up funding from Zhengzhou University. Y.F.H also acknowledges the support from the Xinjiang Tianchi Program.

- 
- [1] B. P. Abbott and et al. (LIGO Scientific Collaboration and Virgo Collaboration), *Phys. Rev. Lett.* **119**, 161101 (2017).
- [2] B. P. Abbott and et al. (LIGO Scientific Collaboration and Virgo Collaboration), *Astrophys. J. Lett.* **848**, L12 (2017).
- [3] B. Margalit and B. D. Metzger, *Astrophys. J. Lett.* **850**, L19 (2017).
- [4] A. Bauswein, O. Just, H.-T. Janka, and N. Stergioulas, *Astrophys. J. Lett.* **850**, L34 (2017).
- [5] M. Shibata, S. Fujibayashi, K. Hotokezaka, K. Kiuchi, K. Kyutoku, Y. Sekiguchi, and M. Tanaka, *Phys. Rev. D* **96**, 123012 (2017).
- [6] E. Annala, T. Gorda, A. Kurkela, and A. Vuorinen, *Phys. Rev. Lett.* **120**, 172703 (2018).
- [7] F. J. Fattoyev, J. Piekarewicz, and C. J. Horowitz, *Phys. Rev. Lett.* **120**, 172702 (2018).
- [8] V. Paschalidis, K. Yagi, D. Alvarez-Castillo, D. B. Blaschke, and A. Sedrakian, *Phys. Rev. D* **97**, 084038 (2018).
- [9] E.-P. Zhou, X. Zhou, and A. Li, *Phys. Rev. D* **97**, 083015 (2018).
- [10] M. Ruiz, S. L. Shapiro, and A. Tsokaros, *Phys. Rev. D* **97**, 021501(R) (2018).
- [11] D. Radice, A. Perego, F. Zappa, and S. Bernuzzi, *Astrophys. J. Lett.* **852**, L29 (2018).
- [12] L. Rezzolla, E. R. Most, and L. R. Weih, *Astrophys. J. Lett.* **852**, L25 (2018).
- [13] R. Nandi and P. Char, *Astrophys. J.* **857**, 12 (2018).
- [14] Z.-Y. Zhu, E.-P. Zhou, and A. Li, *Astrophys. J.* **862**, 98 (2018), arXiv:1802.05510.
- [15] S. Ai, H. Gao, Z.-G. Dai, X.-F. Wu, A. Li, B. Zhang, and M.-Z. Li, *Astrophys. J.* **860**, 57 (2018), arXiv:1802.00571.
- [16] Y.-L. Ma, H. K. Lee, W.-G. Paeng, and M. Rho, *Sci. China Phys. Mech.* **62**, 1 (2019).
- [17] C. Zhang, *Phys. Rev. D* **101**, 043003 (2020).
- [18] C.-M. Li, S.-Y. Zuo, Y. Yan, Y.-P. Zhao, F. Wang, Y.-F. Huang, and H.-S. Zong, *Phys. Rev. D* **101**, 063023 (2020).
- [19] Z. Miao, J.-L. Jiang, A. Li, and L.-W. Chen, *Astrophys. J. Lett.* **917**, L22 (2021).
- [20] H. Tan, V. Dexheimer, J. Noronha-Hostler, and N. Yunes, *Phys. Rev. Lett.* **128**, 161101 (2022).
- [21] Z.-C. Zou and Y.-F. Huang, *Astrophys. J. Lett.* **928**, L13 (2022).
- [22] C.-M. Li, S.-Y. Zuo, Y.-P. Zhao, H.-J. Mu, and Y.-F. Huang, *Phys. Rev. D* **106**, 116009 (2022).
- [23] C. Zhang, Y. Gao, C.-J. Xia, and R. Xu, *Phys. Rev. D* **108**, 063002 (2023).
- [24] J. M. Lattimer and M. Prakash, *Science* **304**, 536 (2004).
- [25] J. Lattimer, *Ann. Rev. Nucl. Part. Sci.* **71**, 433 (2021).
- [26] F. Özel and P. Freire, *Annu. Rev. Astron. Astr.* **54**, 401 (2016).
- [27] S. Goriely, N. Chamel, and J. M. Pearson, *Phys. Rev. C* **82**, 035804 (2010).
- [28] N. Chamel, A. F. Fantina, J. M. Pearson, and S. Goriely, *Phys. Rev. C* **84**, 062802 (2011).
- [29] Fantina, A. F., Chamel, N., Pearson, J. M., and Goriely, S., *A&A* **559**, A128 (2013).
- [30] E. Giliaberti and G. Cambiotti, *Mon. Not. Roy. Astron. Soc.* **511**, 3365 (2022).
- [31] Fantina, A. F., Zdunik, J. L., Chamel, N., Pearson, J. M., Suleiman, L., and Goriely, S., *A&A* **665**, A74 (2022).
- [32] S. P. Klevansky, *Rev. Mod. Phys.* **64**, 649 (1992).
- [33] M. Buballa, *Phys. Rep.* **407**, 205 (2005).
- [34] Z. Li, K. Xu, X. Wang, and M. Huang, *Eur. Phys. J. C* **79**, 245 (2019).
- [35] J. Liu, Y. Du, and S. Shi, *Symmetry* **13** (2021).
- [36] J.-L. Zhang, G.-Z. Kang, and J.-L. Ping, *Phys. Rev. D* **105**, 094015 (2022).
- [37] M. Huang and P. Zhuang, *Symmetry* **15** (2023).

- [38] A. Ayriyan, D. Blaschke, A. G. Grunfeld, D. Alvarez-Castillo, H. Grigorian, and V. Abgaryan, *Eur. Phys. J. A* **57**, 318 (2021).
- [39] D. Blaschke, A. Ayriyan, D. E. Alvarez-Castillo, and H. Grigorian, *Universe* **6** (2020), 10.3390/universe6060081.
- [40] D. Alvarez-Castillo, A. Ayriyan, S. Benic, D. Blaschke, H. Grigorian, and S. Typel, *Eur. Phys. J. A* **52**, 1 (2016).
- [41] A. Pfaff, H. Hansen, and F. Gulminelli, *Phys. Rev. C* **105**, 035802 (2022).
- [42] T. Endo, T. Maruyama, S. Chiba, and T. Tatsumi, *Prog. Theor. Phys.* **115**, 337 (2006).
- [43] M. Hempel, G. Pagliara, and J. Schaffner-Bielich, *Phys. Rev. D* **80**, 125014 (2009).
- [44] N. Yasutake, T. Maruyama, and T. Tatsumi, *Phys. Rev. D* **80**, 123009 (2009).
- [45] N. K. Glendenning, *Phys. Rev. D* **46**, 1274 (1992).
- [46] A. Bhattacharyya, I. N. Mishustin, and W. Greiner, *J. Phys. G: Nucl. Part. Phys.* **37**, 025201 (2010).
- [47] F. Özel, *Nature* **441**, 1115 (2006).
- [48] C. Hoyos, N. Jokela, D. Rodríguez Fernández, and A. Vuorinen, *Phys. Rev. Lett.* **117**, 032501 (2016).
- [49] P. Qin, Z. Bai, S. Wang, C. Wang, and S.-x. Qin, *Phys. Rev. D* **107**, 103009 (2023).
- [50] G. Baym, T. Hatsuda, T. Kojo, P. D. Powell, Y. Song, and T. Takatsuka, *Rep. Prog. Phys.* **81**, 056902 (2018).
- [51] K. Masuda, T. Hatsuda, and T. Takatsuka, *Astrophys. J* **764**, 12 (2013).
- [52] K. Masuda, T. Hatsuda, and T. Takatsuka, *Prog. Theor. Exp. Phys.* **2013** (2013), 10.1093/ptep/ptt045.
- [53] T. Kojo, P. D. Powell, Y. Song, and G. Baym, *Phys. Rev. D* **91**, 045003 (2015).
- [54] C.-M. Li, J.-L. Zhang, T. Zhao, Y.-P. Zhao, and H.-S. Zong, *Phys. Rev. D* **95**, 056018 (2017).
- [55] C.-M. Li, J.-L. Zhang, Y. Yan, Y.-F. Huang, and H.-S. Zong, *Phys. Rev. D* **97**, 103013 (2018).
- [56] C.-M. Li, Y. Yan, J.-J. Geng, Y.-F. Huang, and H.-S. Zong, *Phys. Rev. D* **98**, 083013 (2018).
- [57] B.-L. Li, Y. Yan, and J.-L. Ping, *J. Phys. G: Nucl. Part. Phys.* **49**, 045201 (2022).
- [58] J. Antoniadis, P. C. C. Freire, N. Wex, T. M. Tauris, R. S. Lynch, M. H. van Kerkwijk, M. Kramer, C. Bassa, V. S. Dhillon, T. Driebe, J. W. T. Hessels, V. M. Kaspi, V. I. Kondratiev, N. Langer, T. R. Marsh, M. A. McLaughlin, T. T. Pennucci, S. M. Ransom, I. H. Stairs, J. van Leeuwen, J. P. W. Verbiest, and D. G. Whelan, *Science* **340**, 1233232 (2013).
- [59] H. T. Cromartie, E. Fonseca, S. M. Ransom, P. B. Demorest, Z. Arzoumanian, H. Blumer, P. R. Brook, M. E. DeCesar, T. Dolch, J. A. Ellis, *et al.*, *Nat. Astron.* **4**, 72 (2020).
- [60] B. P. Abbott and et al. (The LIGO Scientific Collaboration and the Virgo Collaboration), *Phys. Rev. Lett.* **121**, 161101 (2018).
- [61] T. E. Riley, A. L. Watts, S. Bogdanov, P. S. Ray, R. M. Ludlam, S. Guillot, S. Arzoumanian, C. L. Baker, A. V. Bilous, D. Chakrabarty, K. C. Gendreau, A. K. Harding, W. C. G. Ho, J. M. Lattimer, S. M. Morsink, and T. E. Strohmayer, *Astrophys. J. Lett.* **887**, L21 (2019).
- [62] M. C. Miller, F. K. Lamb, A. J. Dittmann, S. Bogdanov, Z. Arzoumanian, K. C. Gendreau, S. Guillot, A. K. Harding, W. C. G. Ho, J. M. Lattimer, R. M. Ludlam, S. Mahmoodifar, S. M. Morsink, P. S. Ray, T. E. Strohmayer, K. S. Wood, T. Enoto, R. Foster, T. Okajima, G. Prigozhin, and Y. Soong, *Astrophys. J. Lett.* **887**, L24 (2019).
- [63] T. E. Riley, A. L. Watts, P. S. Ray, S. Bogdanov, S. Guillot, S. M. Morsink, A. V. Bilous, Z. Arzoumanian, D. Choudhury, J. S. Deneva, K. C. Gendreau, A. K. Harding, W. C. G. Ho, J. M. Lattimer, M. Loewenstein, R. M. Ludlam, C. B. Markwardt, T. Okajima, C. Prescod-Weinstein, R. A. Remillard, M. T. Wolff, E. Fonseca, H. T. Cromartie, M. Kerr, T. T. Pennucci, A. Parthasarathy, S. Ransom, I. Stairs, L. Guillemot, and I. Cognard, *Astrophys. J. Lett.* **918**, L27 (2021).
- [64] M. C. Miller, F. K. Lamb, A. J. Dittmann, S. Bogdanov, Z. Arzoumanian, K. C. Gendreau, S. Guillot, W. C. G. Ho, J. M. Lattimer, M. Loewenstein, S. M. Morsink, P. S. Ray, M. T. Wolff, C. L. Baker, T. Cazeau, S. Manthripragada, C. B. Markwardt, T. Okajima, S. Pollard, I. Cognard, H. T. Cromartie, E. Fonseca, L. Guillemot, M. Kerr, A. Parthasarathy, T. T. Pennucci, S. Ransom, and I. Stairs, *Astrophys. J. Lett.* **918**, L28 (2021).
- [65] A. Bauswein, N.-U. F. Bastian, D. B. Blaschke, K. Chatziioannou, J. A. Clark, T. Fischer, and M. Oertel, *Phys. Rev. Lett.* **122**, 061102 (2019).
- [66] Z. Miao, A. Li, Z. Zhu, and S. Han, *Astrophys. J* **904**, 103 (2020).
- [67] B. Holdom, J. Ren, and C. Zhang, *Phys. Rev. Lett.* **120**, 222001 (2018).
- [68] E. Laermann and O. Philipsen, *Ann. Rev. Nucl. Part. Sci.* **53**, 163 (2003).
- [69] D. Alvarez-Castillo, A. Ayriyan, G. G. Barnaföldi, H. Grigorian, and P. Pósfay, *Eur. Phys. J. Spec. Top.* **229**, 3615 (2020).
- [70] A. Ayriyan, D. Alvarez-Castillo, D. Blaschke, and H. Grigorian, *Universe* **5** (2019), 10.3390/universe5020061.
- [71] A. Ayriyan, D. E. Alvarez-Castillo, D. Blaschke, H. Grigorian, and M. Sokolowski, *Phys. Part. Nucl.* **46**, 854 (2015).
- [72] M. C. Miller, C. Chirenti, and F. K. Lamb, *Astrophys. J* **888**, 12 (2019).
- [73] Particle Data Group, R. Workman, V. Burkert, and et al., *Prog. Theor. Exp. Phys.* **2022**, 083C01 (2022).
- [74] Z.-F. Cui, S.-S. Xu, B.-L. Li, A. Sun, J.-B. Zhang, and H.-S. Zong, *Eur. Phys. J. C* **78**, 770 (2018).
- [75] S.-S. Xu, Z.-F. Cui, A. Sun, and H.-S. Zong, *J. Phys. G: Nucl. Part. Phys.* **45**, 105001 (2018).
- [76] C.-M. Li, P.-L. Yin, and H.-S. Zong, *Phys. Rev. D* **99**, 076006 (2019).
- [77] Z. Hong-Shi and S. Wei-Min, *Commun. Theor. Phys.* **46**, 717 (2006).
- [78] L. Reinders, H. Rubinstein, and S. Yazaki, *Phys. Rep.* **127**, 1 (1985).
- [79] T. G. Steele, *Z. Phys. C* **42**, 499 (1989).
- [80] P. Pascual and R. Tarrach, *QCD: Renormalization for the Practitioner* (Springer, 1984).
- [81] Y. Jiang, H. Gong, W.-M. Sun, and H.-S. Zong, *Phys. Rev. D* **85**, 034031 (2012).
- [82] Z.-F. Cui, C. Shi, Y.-H. Xia, Y. Jiang, and H.-S. Zong, *Eur. Phys. J. C* **73**, 2612 (2013).
- [83] Z.-F. Cui, C. Shi, W.-M. Sun, Y.-L. Wang, and H.-S. Zong, *Eur. Phys. J. C* **74**, 2782 (2014).
- [84] C. Shi, Y.-L. Du, S.-S. Xu, X.-J. Liu, and H.-S. Zong, *Phys. Rev. D* **93**, 036006 (2016).

- [85] Q.-W. Wang, Z.-F. Cui, and H.-S. Zong, *Phys. Rev. D* **94**, 096003 (2016).
- [86] Z.-Y. Fan, W.-K. Fan, Q.-W. Wang, and H.-S. Zong, *Mod. Phys. Lett. A* **32**, 1750107 (2017).
- [87] W. Fan, X. Luo, and H. Zong, *Chin. Phys. C* **43**, 054109 (2019).
- [88] Y.-L. Du, Z.-F. Cui, Y.-H. Xia, and H.-S. Zong, *Phys. Rev. D* **88**, 114019 (2013).
- [89] J.-L. Zhang, Y.-M. Shi, S.-S. Xu, and H.-S. Zong, *Mod. Phys. Lett. A* **31**, 1650086 (2016).
- [90] H. Kohyama, D. Kimura, and T. Inagaki, *Nucl. Phys. B* **896**, 682 (2015).
- [91] H.-S. Zong and W.-M. Sun, *Int. J. Mod. Phys. A* **23**, 3591 (2008).
- [92] Y. Yan, J. Cao, X.-L. Luo, W.-M. Sun, and H.-S. Zong, *Phys. Rev. D* **86**, 114028 (2012).
- [93] O. G. Benvenuto and G. Lugones, *Phys. Rev. D* **51**, 1989 (1995).
- [94] D. Lu, K. Tsushima, A. Thomas, A. Williams, and K. Saito, *Nucl. Phys. A* **634**, 443 (1998).
- [95] G. Song, W. Enke, and L. Jiarong, *Phys. Rev. D* **46**, 3211 (1992).
- [96] T. Hinderer, B. D. Lackey, R. N. Lang, and J. S. Read, *Phys. Rev. D* **81**, 123016 (2010).